National Conference on Failure Analysis – 2006, Hyderabad, 22-23rd Dec'06: Organised by DMRL-Hyderabad, NAL-Bangalore, IGCAR-Kalpakkam, CMAC-Bangalore and IIM-Hyderabad Chapter

INVESTIGATION OF CAVING-IN INCIDENT OF MIG 21 AIRCRAFT

M. Ghosh, S. K. Das and S. R. Singh
Scientist, Materials Science & Technology Division
National Metallurgical Laboratory (CSIR), Jamshedpur-831007
Ph: (0657) 2270027, e-mail: mainakg@nmlindia.org, srsingh@nmlindia.org

ABSTRACT

In an accident, the starboard (STBD) side of front fuselage was 'caved in' during ground run of the Mig-21. A post-incident inspection revealed vertical and horizontal cracking occurred at the edges of the additional air intake shutter (AAITS). The guard of the AAITS was sucked in causing extensive damage to the aeroengine. However, port side fuselage remained un-affected.
The chemical composition and evaluation of the mechanical properties of the alloy match with the Russian specification D16AT, D16ATB. It means that the duralumin alloy is in hardened and aged condition. Characterization of microstructure in optical, SEM and TEM illustrate more or less negligible variation for fresh and service exposed material.
From the investigation it can be inferred, on the starboard side near some of the rivet holes at the edges of AAITS opening, primary cracks were formed owing to fretting fatigue. The structural non-uniformity of annular area on the starboard side with respect to port side raised the air pressure around the frame #5 and the skin 'caved-in'. As engine demanded more air, under severe suction pressure, the skin containing micro-cracks became unable to withstand the load and the guard was sucked in from outside towards the engine causing overload failure to the areas away from rivet hole and rest of the zones near the AAITS.

INTRODUCTION

Presently, life extension study of MIG-21 aircraft is undertaken by concerned government agencies. This includes full scale fatigue testing of the aircraft. However, in a combat sortie, a MIG-21 aircraft was initially pulled 8.5G in air and subsequently was inducted for high 'G' checks. During the ground run after warming up at 90%, engine was accelerated to maximum rating (100%). A loud bang was heard immediately and the engine was cut off at the same moment. A post-incident inspection revealed, that starboard side structure (STBD) between frame 3 and 10 had caved-in (~30mm). Vertical and horizontal cracking were found at the edges of the additional air intake shutter (AAITS). The guard of the AAITS was sucked in causing extensive damage to the aeroengine. Yet, port side fuselage remained un-affected. An annular area along the plane of lip for starboard side was found to be 30.9cm^2 lesser than port side region. Theoretical calculation on nominal and minimal accepted annular areas revealed, that port side area is within the accepted limit, whereas starboard side was not.

Hence, the present investigation aims at examining the 'caved in' structure in details to explore the root cause of failure; i.e., whether it is owing to heterogeneity of the supplied material or degeneration of the alloy due to service exposure or pre-existing fatigue cracking in the fuselage or due to some other reason.

EXPERIMENTAL

The affected regions of the 'caved-in' MIG-21 are shown in Fig.1a with the sampling locations in Fig.1b. The sample designation is given in Table-1.

Table-1: Samples for microstructural characterization.

Material designation	Sample I.D	Sr. No.	Location
Un-exposed fresh sheet.	Sample A1	1	Longitudinal section i.e. along rolling direction.
	Sample A2		Transverse section i.e. perpendicular to rolling direction.
Service exposed, L.H, additional air in-take shutter, frame #9; unaffected.	Sample B1	4	Longitudinal section i.e. along rolling direction.
	Sample B2		Transverse section i.e. perpendicular to rolling direction.
Service exposed, R.H, frame #5.	Sample C1	3	Longitudinal section i.e. along rolling direction.
	Sample C2		Transverse section i.e. perpendicular to rolling direction.
Service exposed, R.H, frame #9; cracked.	Sample D1	2	Longitudinal section i.e. along rolling direction.
	Sample D2		Transverse section i.e. perpendicular to rolling direction.

The Bulk chemical composition of the alloy was determined in optical emission spectrometer (PMI-Master Plus). Samples for structural characterization were mounted and prepared by conventional metallographic technique and etched with Keller's reagent (2ml HF, 3ml HCl, 5ml HNO_3 and 190ml H_2O). The etched specimen was observed in optical microscope (Correct SDME TR5) and in scanning electron microscope (SEM, Jeol JSM 840A). Energy dispersive spectrometer (Kevex) was used to determine the chemical composition of micro constituents. Hardness of the samples was determined in Vickers scale at 10Kgf load (AFFRI, VRSD 270).

Cleaning in ultrasonic bath, the fracture surfaces were observed in SEM using secondary electron to identify the mode/mechanism of fracture/cracking. Tensile testing was carried out at a $3.3x10^{-4}$ sec^{-1} strain rate as per ASTM specification (Vol.03.01:E8M-96) having 50mm gauge length and 12.5mm width to evaluate 0.2% off set yield, UTS and fracture strain in Instron. Reproducibility was also checked by repeating the test for three samples for each type of specimen.

Samples were also characterized in transmission electron microscopy to explore sub-microscopic microstructural features. The sheets were mechanically thinned down to the thickness of ~0.1mm, punched to make 3mm diameter discs and further thinned down to electron transparency in twin jet electro polisher (Fischione, model 120) using ethanol and perchloric acid mixture (90:10) as an electrolyte at -10^{o}C and 15V potential. The samples were observed in transmission electron microscope (Philips, CM-200) at an operating voltage of 200kV.

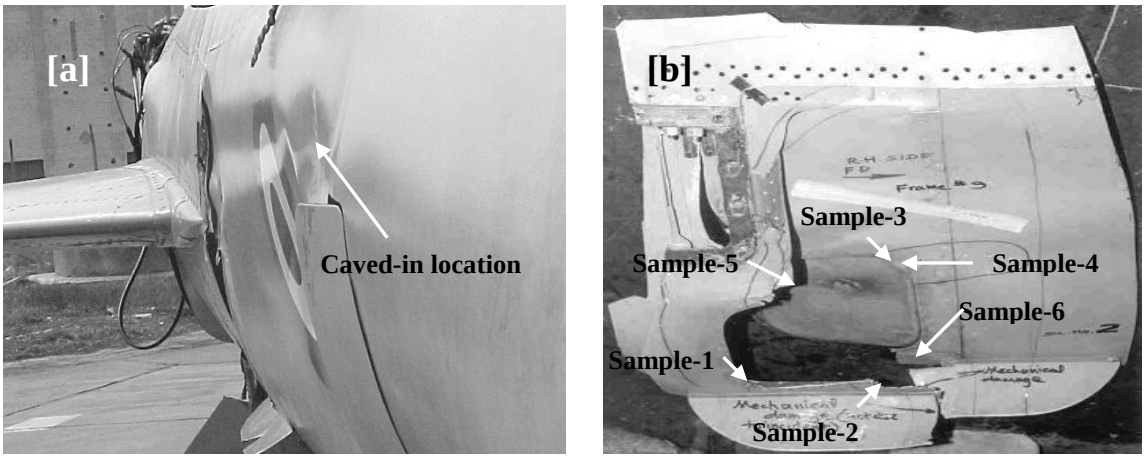

Figs.1 (a & b): Photographs of 'caved in' MIG-21 aircraft [a] 'caved in' location at anti surge shutter, [b] multiple crack formation near additional air intake shutter and sampling location for fractography.

RESULTS AND DISCUSSION

The chemical composition of the alloy is collated in table-2.

Table-2: Chemical composition of the alloy (wt%).

Alloying elements	As per Russian specification	Chemical analysis		
		Sample A	Sample C	Sample D
Cu	3.8-4.9	4.67	4.52	4.68
Mg	1.2-1.8	1.41	1.21	1.37
Mn	0.3-0.9	0.67	0.46	0.52
Al	Bal	Bal	Bal	Bal
Fe	0.5 max	0.45	0.53	0.45
Si	0.5 max	0.24	0.29	0.26
Zn	0.3 max	0.07	0.21	0.14
Ni	0.1 max	0.0123	0.0341	0.0389
Others total	-	0.0849	0.0905	0.0737
Total admixture	1.50 max	0.5739	0.6829	0.5882

The nearest Russian specification of the given material is D16AT/ D16ATB duralumin alloy. The above specification is also close to Indian specification of 24345 IS 3436.

The optical (Fig.2a to d) and scanning electron micrographs (Fig.3a & b) of both the as received fresh sheet as well as service exposed sheets exhibit more or less same features. α-Al matrix is decorated with the uniform distribution of second phase. The size of the second phase varies widely and they are preferably orientated along the rolling direction. Two types of precipitates are observed; the larger ~10-14μm and the smaller one < 4μm. The pancake structure of grains due to rolling is evident in the transverse section (Fig.2b & d). The micro-analysis of the precipitates is furnished in Table-3. The precipitates are mainly consists of Al and Cu containing varying amount of Mn, Fe, Ni and Mg.

Table-3: Concentration of alloying elements in the second phases

Sample I.D	**Type of second phase**	**Concentration of alloying elements (%wt)**						
		Al	**Si**	**Mn**	**Fe**	**Cu**	**Ni**	**Mg**
Sample A	Bright large precipitate (I)	30.04	0.51	2.85	6.77	50.84	-	-
Sample D	Large bright precipitate (II)	53.55	-	-	-	45.08	-	1.4

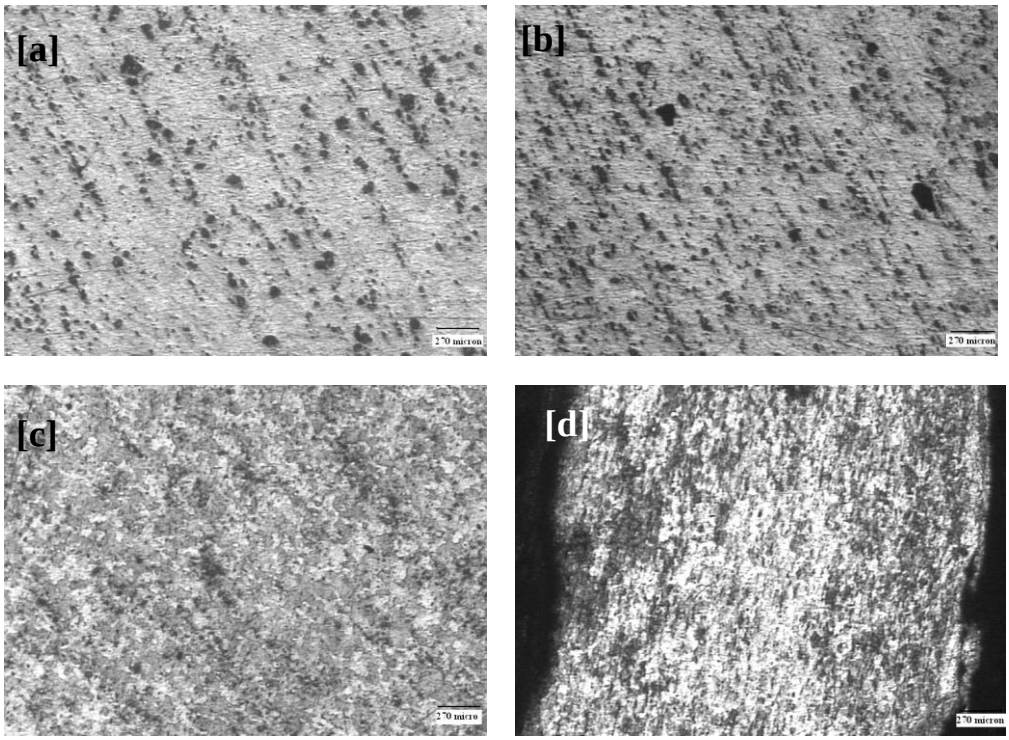

Fig.2 (a,b,c & d): Optical microstructure of specimens showing distribution of second phase in the matrix, [a] and [b] longitudinal and transverse section of sample-A, [c] and [d] longitudinal and transverse section of sample-D respectively.

The hardness of the different sections is collated in Table-4. The hardness varies more or less within the range of 131-136HV; however transverse direction of sample A exhibits higher value (~145HV). The difference in the hardness of sample A in the two directions is due to the existence of larger volume fraction of second phases as well as presence of

larger size precipitate in the transverse direction. On an average the hardness value of the material indicates hardened and naturally aged i.e. T6 heat treatment condition of D16AT/ D16ATB duralumin alloy.

The mechanical properties of the specimens are furnished in Table-5. It has been observed, that the service exposed material 'B' exhibits higher tensile strength and lower elongation with respect to the fresh sheet 'A'. The mechanical properties of both the samples are well above the specification.

Table-4: Hardness of samples in Vickers scale

Sample I.D.	Name of the section	Hardness (HV)
A	Longitudinal	134 ± 2
	Transverse	145 ± 1
B	Longitudinal	132 ± 1
	Transverse	127 ± 1
C	Longitudinal	136 ± 2
	Transverse	131 ± 2
D	Longitudinal	136 ± 1
	Transverse	136 ± 2

In the microstructure, for sample A and B, the precipitate size is more or less same; however in case of the latter the isolated precipitates in the longitudinal direction are larger in size than the second phases of same type in the former. So, a minor difference in the UTS and YS are found for sample B with respect to sample A.

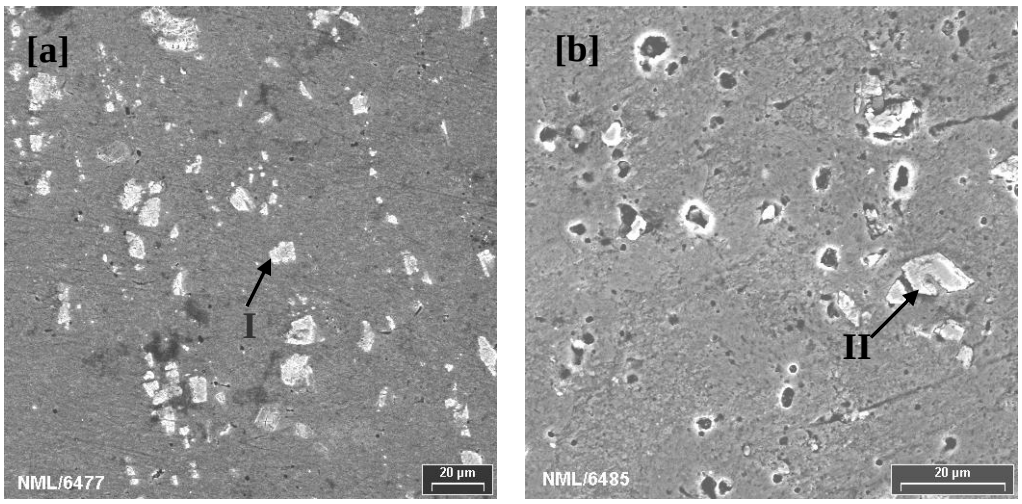

Fig.3 (a & b): SEM micrographs of specimens revealing different types of second phase in the matrix.

Table-5: Mechanical properties of the alloy at ambient temperature

Mechanical poroperties	As per specification	Sample I.D	
		Sample A	Sample B
Ultimate tensile strength (MPA)	426.50	442.7 ± 5	468 ± 3

0.2% Off set yield (MPa)	274.5	367.3 ± 2	370.9 ± 5
Breaking load (MPa)	-	422.4 ± 1	428.3 ± 4
Elongation (%)	13.0	18.1 ± 0.3	16.3 ± 1

The SEM observations of the fracture surfaces of the six samples are shown in Figs. 4, 5, 6 and 7. The fracture region of sample-1 is transgranular cleavage in nature, imprinted with fatigue striations in localized region (Fig.4a). The fatigue crack is pre-existing in nature; however fracture initiated at surface (arrow in Fig.4b) and grows through the thickness direction as well as along the longitudinal direction (along the flight direction).
As the curvature of the skin changes, the mixed direction of the crack propagation becomes prevalent in nature (Fig.4c); the right side curvature appears straight and the left side has got a radius. Fracture surface is covered with oxides at some locations. Adjacent to rivet joint, the fracture surface is shining in nature indicating fatigue failure, where as away from rivet it is dull in appearance indicating secondary dimple fracture owing to overload (Fig.4d). The length of the fatigue zone is ~3.5mm. Secondary cracking is also observed (arrow in Fig.4a).
Sample-2, 3 and 4 mainly exhibit secondary failure characterized by the presence of fine dimples. Rubbing marks due to mechanical damage are also present in the fracture surface and surface is partially covered with oxides.
For sample-5, the fatigue failure initiated at the rivet hole (arrow in Fig.1b) having a length of ~3mm. Machining marks are found near the hole on the left side (Fig.5a). Two main cracks are found on the fracture surface (Fig.5a); one is horizontal (over the surface of the skin, moving towards the flight direction) and the other one i.e. the main crack moves vertically downward (along the thickness, perpendicular to the flight direction). Middle of the fracture surface is decorated with fatigue striations along with the existence of secondary cracking (Fig.5a and b).
Fracture surface of sample-6 is the combination of dimples owing to secondary failure near the rivet hole (arrow in Fig.2b) and fatigue striations. However, in this case fatigue failure initiated from second phases embedded inside the sample i.e. somewhere across its thickness (Fig.6a). The length of the fatigue zone is ~800μm. The crack initially moves outward along the thickness direction (perpendicular to flight direction) and propagates along the periphery parallel to flight direction.
The TEM study reveals the sub-microscopic microstructural features present in the alloy. The fresh sheet as well as sample-D contains second phases of ~0.02 μm, well dispersed within α-Al matrix (Fig. 7a). Large second phases like ~0.5μm are also found (Fig.7.b). Planar defects are also observed in these precipitates (Figs.7a). The selected area electron diffraction pattern (SADP) shown in Fig. 7c spot pattern of aluminium matrix and Al_2Cu precipitates. Shape of the precipitates also changes with the service exposure with respect to the fresh sheet as elongated precipitates are found along with the elliptical and spherical precipitates.

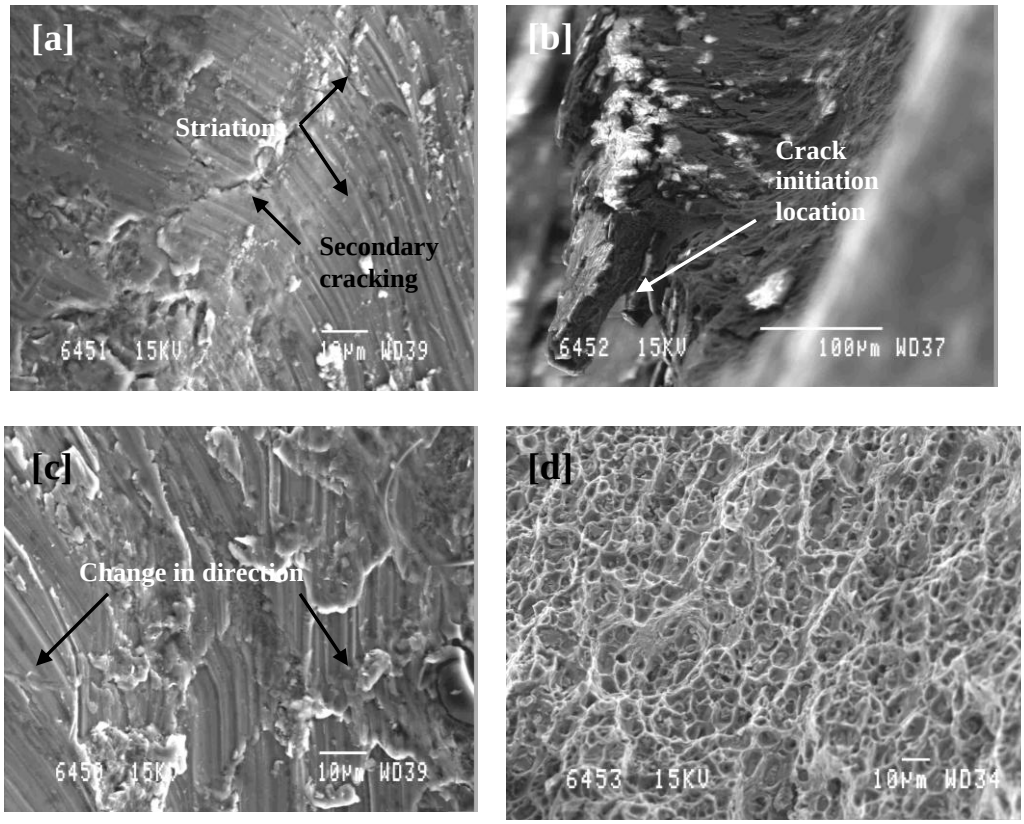

Figs.4 (a,b,c & d): SEM micrographs of Sample-1 revealing fatigue fracture [a] fatigue striations and secondary cracking, [b] fatigue crack initiation location, [c] mixed direction of fatigue striation and [d] dimple fracture.

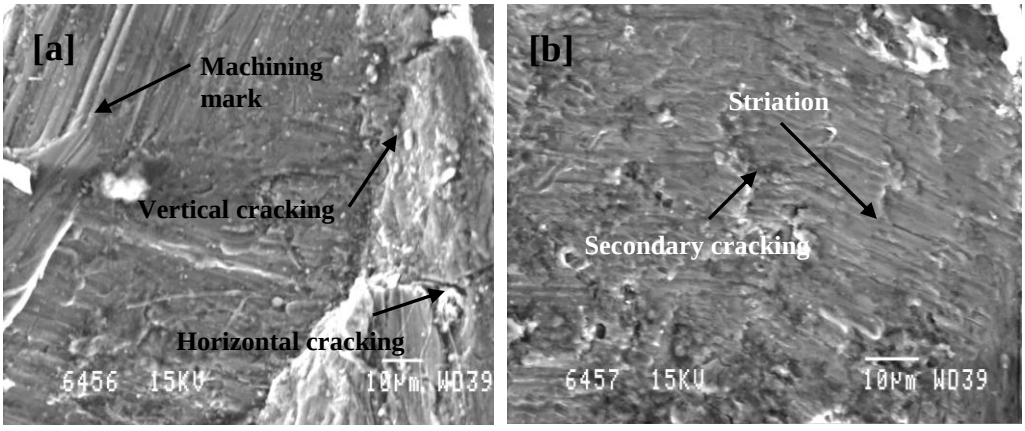

Figs.5 (a & b) : Fractographs of sample-5 showing [a] two different cracks at right angle and [b]striations with secondary cracking.

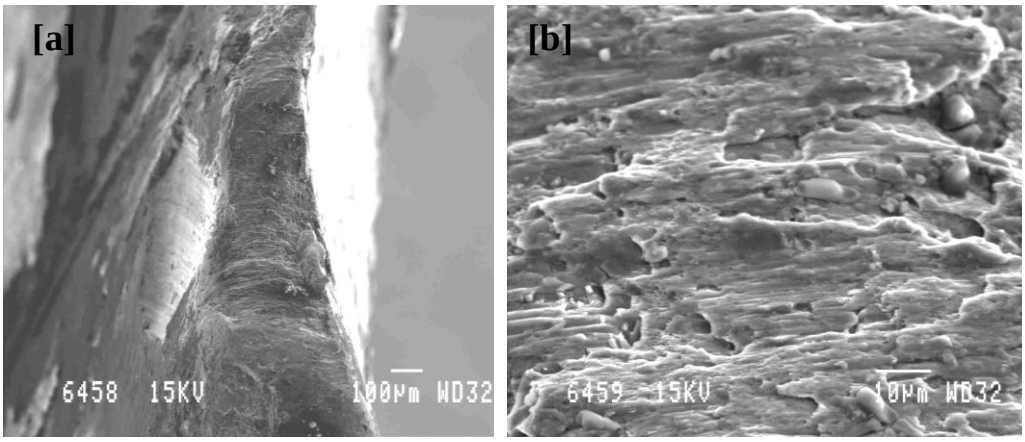

Fig.6 (a & b) : Fracture surface of Sample-6 illustrating [a] fatigue crack initiation location and [b] fatigue striations.

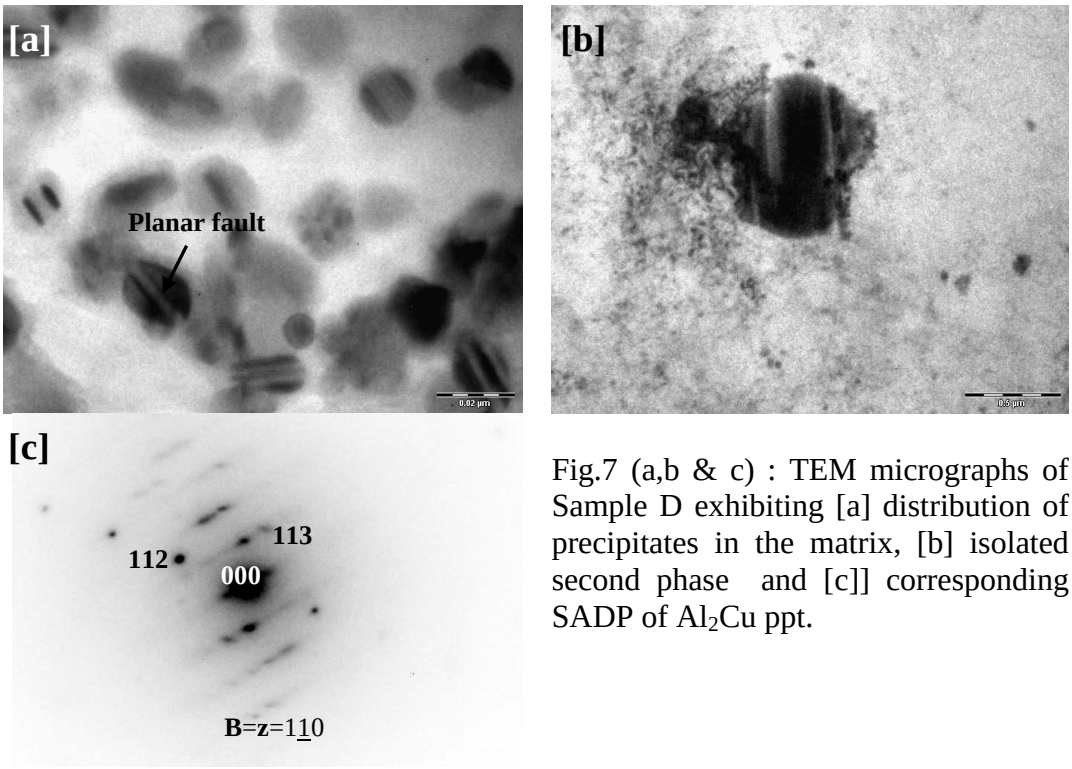

Fig.7 (a,b & c) : TEM micrographs of Sample D exhibiting [a] distribution of precipitates in the matrix, [b] isolated second phase and [c]] corresponding SADP of Al_2Cu ppt.

From the above observations, it is evident that microstructure and mechanical properties of the fresh as well as service exploited material has minimal variation. The presence of cracking is observed for sample 1 and 5 near the rivet hole. These primary cracks are formed perhaps owing to fretting fatigue. This fretting fatigue occurred during service exploitation at those particular locations, where the rivet holes got loosened after a substantial span of time. Moreover, the induced strain due to presence of second phases becomes severe adjacent to the rivet joints. As mentioned earlier, the reduction of annular area of the star board side with respect to port side was also found at the time of

investigation. Air pressure inside the channel of the starboard side is thus reduced owing to less volume fraction of air flow. Under this situation, due to severe outer air pressure, the starboard structure 'caved-in' near frame #5 and causes less air flow to the engine. To propel the aircraft, more air was demanded and the only way was additional air in-take shutter. The air pressure builds up around the AAITS and the pre-existing fatigue cracks at the above locations grows in the direction of high stress gradient (i.e., parallel to flight direction along the periphery) as well as along the thickness direction. The load bearing ability of the skin near AAITS is decreased and the guard was sucked in through that fractured location towards the engine causing overload failure to the rest of the peripheral location of the AAITS and the regions away from rivet hole. Strain hardening due to large size brittle precipitates is also responsible in crack formation as revealed in sample 6.

SUMMARY AND CONCLUSION

The evaluation of its chemical composition and mechanical properties of the material indicate that the alloy is D16AT/D16ATB. It means that the duralumin alloy is in hardened and aged condition.

ii) Microstructural degradation due service exploitation is insignificant and therefore, the possibility of failure due to material is ruled out.

iii) On the starboard side, near some of the rivet holes at the edge of AAITS opening, primary cracks are formed owing to fretting fatigue. Moreover, the structural non-uniformity of annular area on the starboard side with respect to port side causes the air pressure drop inside the air way channel of the starboard side. Thus the skin near frame#5 caved-in owing to imbalance of in and out side air pressure and results in reduction of air flow to engine. Drop in air flow to the engine builds up severe air pressure around the AAITS as engine demanded more and more air and the already cracked skin became unable to bear the load. Naturally the guard was sucked in from outside leading to overload failure to the areas away from rivet hole and rest of the zones near the AAITS.